Effects of drying rate and slurry microstructure on the formation process of LiB cathode and electrochemical properties

Komoda, Yoshiyuki ; Ishibashi, Kaoru ; Kuratani, Kentaro ; Suzuki, Kosuke ; Ohmura, Naoto ; Kobayashi, Hironori

(Citation)
Journal of Power Sources,568:232983

(Issue Date)
2023-06-01

(Resource Type)
journal article

(Version)
Version of Record

Journal of Power Sources 568 (2023) 232983

Contents lists available at ScienceDirect

Journal of Power Sources

journal homepage: www.elsevier.com/locate/jpowsour

Effects of drying rate and slurry microstructure on the formation process of LiB cathode and electrochemical properties

Yoshiyuki Komoda [a,b,*], Kaoru Ishibashi [a], Kentaro Kuratani [c,**], Kosuke Suzuki [a], Naoto Ohmura [a], Hironori Kobayashi [c]

[a] Department of Chemical Science and Engineering, Graduate School of Engineering, Kobe University, 1-1, Rokkodai, Nada-ku, Kobe, Hyogo, 657-8501, Japan
[b] Research Center for Membrane and Film Technology, Kobe University, 1-1, Rokkodai, Nada-ku, Kobe, Hyogo, 657-8501, Japan
[c] Research Institute of Electrochemical Energy, Department of Energy and Environment, National Institute of Advanced Industrial Science and Technology (AIST), 1-8-31, Midorigaoka, Ikeda, Osaka, 563-8577, Japan

HIGHLIGHTS

- The dispersed state of electrode slurry and drying rate affects cell performance.
- The segregation of well-dispersed materials reduced rate performance.
- Poorly dispersed slurry causes material localization and low cycle performance.
- Péclet number is useful to determine the optimal drying condition.

GRAPHICAL ABSTRACT

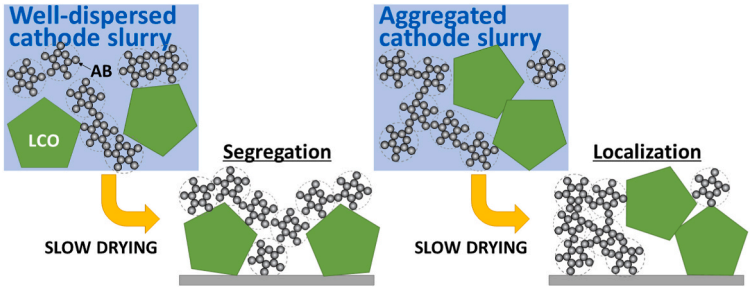

ARTICLE INFO

Keywords:
AB network structure
Particle sedimentation
Packing density
Péclet number

ABSTRACT

The drying process of electrode slurry for LiB should be crucial to obtain higher electrochemical performance, but it has been a black box. Furthermore, the lack of sufficient information on slurry microstructure complicates solving this issue. In this study, the cathode slurries having different internal structures are prepared and characterized by rheological properties. The drying process of the coating layer is evaluated in terms of film shrinkage. When the coarse particles of active material and the network structure of acetylene-black particles are uniformly mixed, a low drying rate results in extensive particle segregation and poor cycle performance. On the other hand, it is found that insufficient dispersion of active materials causes poor rate performance. Under the optimal drying condition, the slurry microstructure is found not to affect battery performance. However, the optimization of drying conditions requires consideration of material mobility during drying.

* Corresponding author. Department of Chemical Science and Engineering, Graduate School of Engineering, Kobe University, 1-1, Rokkodai, Nada-ku, Kobe, Hyogo, 657-8501, Japan.
** Corresponding author.
E-mail addresses: komoda@kobe-u.ac.jp (Y. Komoda), k-kuratani@aist.go.jp (K. Kuratani).

https://doi.org/10.1016/j.jpowsour.2023.232983
Received 18 January 2023; Received in revised form 4 March 2023; Accepted 17 March 2023
Available online 28 March 2023

1. Introduction

The use of battery technology is inevitable to realize a sustainable society worldwide. Lithium-ion batteries (LiBs) have been a leader in battery systems for decades, contributing significantly to developing applications such as laptop computers, smartphones, and electric vehicles. Unfortunately, due to the theoretical limitations of the material, recent LiBs are not expected to make any further significant progress in capacity. Many researchers and engineers have worked to overcome this difficulty by searching for and developing new materials that enable greater capacity and higher current density [1–4]. However, even when such excellent materials are found, many challenges remain in the construction of industrial electrode manufacturing processes, such as mass preparation of highly concentrated electrode slurries, continuous coating of highly viscous slurries, and drying of wide and thick slurry-coated layers. Several recent review papers pointed out the challenges in the manufacturing process [5–9]. So, various state-of-the-art manufacturing techniques have been proposed dramatically improve battery performance [10–12]. In addition, because different materials have different factors that affect the final battery performance, past improvement methods cannot always be adapted as is. Furthermore, operating conditions in the electrode manufacturing process tend to be set on an ad hoc basis. Therefore, conventional lithium-ion battery materials, for which sufficient information on physical and chemical properties has already been reported, are still valuable for systematically investigating the effects of operating conditions in the electrode manufacturing process on the electrode structure.

LiB cathode consists of active materials (AM), conductive additives, and binders. These materials are dispersed in a solvent, coated over an aluminum foil, and dried in an oven to obtain a cathode film. In general, energy density, the amount of electricity stored in a unit volume or weight of a battery cell, is the popular indicator of battery performance. Therefore, the particulate materials must be densely packed as much as possible to reduce the volume of a battery pack and the usage amount of electrolyte. The higher the packing density, the more frequently the materials are connected, thereby reducing electrical resistance. In order to utilize state-of-the-art materials, it is necessary to elucidate the filling process of particulate materials during drying based on scientific knowledge rather than trial and error. Zhang et al. reviewed the mechanism and metrology of the drying process. They emphasized the significance of the three-stage drying model: condensation, void formation, and consolidation [8]. Some studies pointed out that the packing state of AM is mainly determined in the first stage and that the localization of other materials proceeds in the following stages depending on the drying rate [13–17]. However, the mobility of AM must be significantly affected by the surroundings, which is the dispersion of conductive materials, usually showing viscoelastic behavior, and changes with the progress of solvent evaporation. Therefore, the understanding of slurry microstructure and film formation process cannot be discussed separately.

In many cases, AM has a significantly high ability to store electrons but low electrical conductivity. Therefore, it is essential to form a network structure of conductive additives, such as acetylene black (AB) and carbon nanotube (CNT), in the electrode film to transport electrons from the electrode surface to the AM surface. Many researchers have noted that slurry preparation significantly influences electrode conductivity and battery performance [18–22]. Furthermore, we have found that the viscoelastic properties of cathode slurries are affected by that of the AB slurry. The network structure of AB particles, dominating the rheological behavior, depends on the slurry preparation process [23,24]. In order to understand the structural change during the drying of the cathode slurry, we should consider the existence of the network structure of AB particles, which can suppress the packing of AM particles. To accommodate the demand to evaluate the packing behavior, we have so far proposed the measurement of the thickness decrease of coating layers and the methods to analyze the results [25–27]. In the present study, we investigated the effects of the slurry preparation process and the drying temperature on the shrinkage behavior of the coating layer of the cathode slurry during drying. The results highlight the influence of the solvent evaporation rate and the particle network structure on the particle packing behavior. They are expected to provide valuable knowledge for obtaining high-packing density electrodes.

2. Experimental

2.1. Slurry preparation and characterization

A cathode slurry used in this study is composed of active materials (Lithium Cobalt Oxide, LCO, 6.8 μm, 5.05 g/ml), conductive additives (Acetylene Black, AB, 35 nm, 2.2 g/ml), binder (Polyvinyldifluoride, PVdF, 1.77 g/ml), and solvent (N-methyl pyrrolidone, NMP, 1.03 g/ml). PVdF was added as 12 wt% NMP solution and finally diluted to 8 wt% by adding NMP as a diluent. Table 1 provides the specific composition.

We have already reported that the slurry preparation process affected the internal structure of the cathode slurry, which can be characterized by rheological measurements. The control of the dispersion state of AB particles is key to obtaining an electrode exhibiting better electrochemical performance because the network structure of AB particles was formed in cathode slurry and contributes to forming electric conductive paths in the electrode after drying. Two different slurry preparation processes were employed to obtain cathode slurry having different AB network structures, as illustrated in Fig. 1. The first is an “in-whole process,” in which all materials, including diluent NMP, are mixed once, and the dispersion operation is repeated six times. Our previous studies have shown that LCO particles cannot penetrate the AB network structure formed in the slurry, and the network structure is hardly destroyed. Another method was the so-called “in-parts process,” where a highly concentrated cathode slurry was first prepared using other than diluent NMP. Then, the NMP addition and dispersion operation were alternately repeated five times. The narrow distance between the LCO particles and the high viscosity allows considerable shear stress to act, which allows the LCO particles to penetrate and break into the network of AB particles, resulting in a cathode slurry with properly dispersed AB particles in the end.

A planetary centrifugal mixer (AR-310, Tinky) was used and operated at 2000 rpm for 3 min for each mixing operation. Rheological properties were measured at room temperature using a stress-controlled rheometer (MCR 301, Anton Paar) equipped with a cone plate fixture (50 mm). Either LCO or AB slurry was prepared through the “in-whole” process; LCO slurry is a mixture of LCO particles and 8 wt% PVdF solution, and AB slurry is a mixture of AB particles and the same binder solution.

2.2. Evaluation of the drying process of a coating layer

The cathode slurry was coated on an aluminum foil, which is adhered to a glass plate, at a coating speed of 6 mm/s using a doctor blade with a

Table 1
Slurry compositions.

	Cathode slurry		LCO slurry	AB slurry
	wt.%	vol.%	vol.%	vol.%
LCO	54.0	20.2	20.6	
AB	2.2	1.9		2.3
PVdF	3.5	3.7	3.8	4.7
NMP	40.4	74.2	75.6	93.0

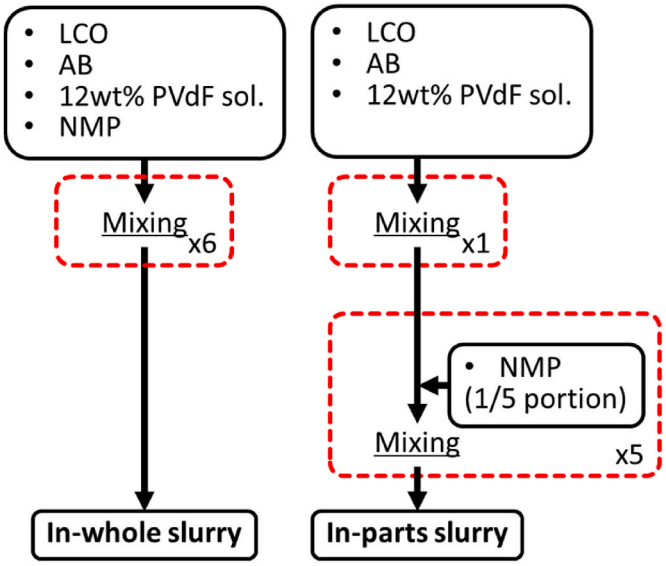

Fig. 1. Preparation process of cathode slurry.

coating gap of 200 μm. The glass plate coated with the slurry was placed on a flat glass heater whose surface temperature was controlled at 45, 80, or 100 °C. Then, as done in our previous studies [25–27], the surface position at the center of the coating layer was measured using a laser displacement sensor (LT-9510, Keyence) with a time interval of 1 s and a resolution of 10 nm. As shown in Fig. 2, the glass plate coated with slurry, the glass heater, and the motorized stage with the laser displacement sensor attached were all placed on a flat hood that allowed NMP vapor to be removed from the bottom. Temperature and humidity-controlled air (25 °C, 50% RH) was supplied into a chamber on the hood surrounding all equipment. After the residual solvent was removed entirely from the coating layer on the glass heater, the final weight was measured on an electric balance.

2.3. Preparation of cells and electrochemical test

Coin-type HS-flat cells from Hohsen Corp. Were assembled in an Ar-filled glove box with the electrodes prepared in §2.2 and lithium foil (Honjo metal) as a counter electrode. A polypropylene sheet and glass filter were used as separators. The cell was sealed after filling the electrolyte solution (1.0 mol dm^{-3} LiPF6 in the 1:1 vol mixture of ethylene carbonate and dimethylene carbonate purchased from Kishida Chemical). The electrochemical properties were examined using a computer-controlled charge and discharge system (BTS-2004, Nagano Co Ltd.). The galvanostatic charge and discharge tests were performed in the cell voltage range of 3.2–4.2 V (vs. Li^+/Li) 100 times at the current densities of 0.1C, corresponding to one discharge or one charge performed in 10 h. The charge and discharge tests were conducted at different current densities of 0.1, 0.5, 1, and 2 C. All measurements were carried out at 30 °C.

3. Results and discussion

3.1. Rheological characterization of cathode slurries

Because viscosity measurement requires that the sample be subjected to shear flow, the internal structure predicted from viscosity may differ from the structure formed in a slurry at rest, corresponding to the coated slurry being dried. For this reason, it is more appropriate to use the frequency dependence of the storage and loss moduli in the linear viscoelastic region where the internal structure is retained. Fig. 3 shows the results for in-whole and in-parts cathode slurries. The cathode slurry can be viewed as a mixture of LCO particles and AB slurry, represented as red dashed lines. Suppose the LCO particles do not enter into the AB network structure in the cathode slurry. In that case, they increase the effective solid volume fraction, which increases the loss modulus. However, the storage modulus derived from the AB network structure remains unchanged. Therefore, the increase in the loss modulus of the cathode slurry can be estimated using the Krieger-Dougherty (K-D) equation [28] as well as viscosity. A solid red curve represents the loss modulus estimate for the cathode slurry.

Indeed, the storage modulus of the in-whole slurry is consistent with that of the AB slurry. The K-D equation could predict its loss modulus. The fact indicates that the AB network structure in the in-whole cathode slurry is equivalent to that of the slurry of AB alone and that no LCO particles can penetrate the AB network structure. Conversely, the loss modulus of the in-parts slurry agrees well with that of the AB slurry at low frequencies. The storage modulus is significantly smaller than that of the AB slurry. The results suggest that LCO particles are embedded in the AB network structure not to increase the effective solid volume fraction and that the destruction of the AB network structure by coarse LCO particles reduces the storage modulus. We conclude from the rheological investigation that LCO particles and large AB network units are independently dispersed in the in-whole slurry. In contrast, LCO particles and smaller AB network units are uniformly mixed on a microscopic scale in the in-parts slurry. Therefore, it can be expected that the in-parts slurry will produce a cathode that exhibits better electrical conductivity.

3.2. Shrinkage behavior of coated slurry

3.2.1. Typical drying behavior and dimensionless expression

The initial weight of the coated slurry, calculated from the final weight after drying and the slurry composition, was converted to the initial thickness using the initial slurry density and coating area. This initial thickness was combined with the variation in surface position measured with the laser displacement sensor to obtain the film thickness

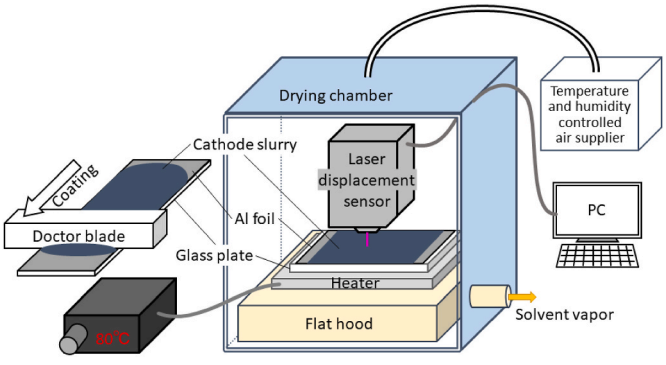

Fig. 2. Experimental setup for measuring the shrinkage of a coating layer.

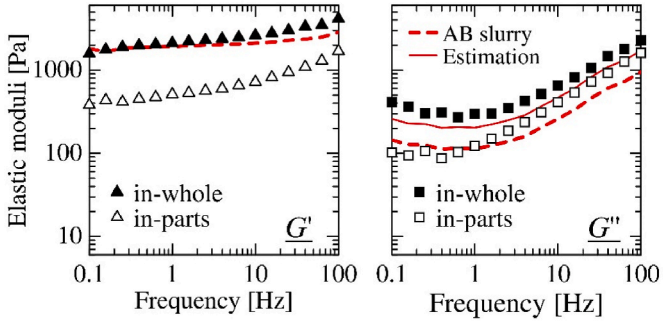

Fig. 3. Viscoelastic behavior of cathode slurries prepared by different processes.

variation during drying. The top graph in Fig. 4 is a typical result showing the shrinkage behavior of the coated cathode slurry. The thickness decreases at a constant rate in the early stages of drying. This decreasing slope of thickness, referred to as shrinkage rate, corresponds to the evaporation rate of NMP from the PVdF solution in the early drying phase. Since the evaporation of NMP is inhibited when particles are densely packed, the particles remain well separated from each other at this stage. Thus, the slurry is concentrated at this stage. In the next stage, however, the decrease in thickness became slower and eventually converged to a constant value. The stable thickness is much larger than the thickness corresponding to the total amount of non-volatile components (LCO, AB, PVdF). In other words, the coated cathode slurry becomes porous during this period. We refer to this stage as the void formation period. These are the first and second of the popular three-stage model [8].

Since the time required to dry the coated slurry depends on the drying temperature and initial thickness, we normalized both axes (time and thickness) of the upper graph in Fig. 4 to obtain the lower graph to discuss the effect of drying conditions on the film shrinkage behavior. First, the thickness was converted to shrinkage ratio $\lambda(t)$ by dividing it by the initial value. Since the coated slurry becomes porous after drying, the final shrinkage ratio is much larger than 0.258, the volume fraction of NV. The solid volume fraction $\varphi(t)$ of the coated slurry during drying is calculated as $\varphi_0/\lambda(t)$, using the initial solid volume fraction φ_0. Note that $1-\varphi(t)$ is the liquid volume fraction during the concentration period and gradually changes to the void fraction during the void formation period. On the other hand, the elapsed time from the start of drying was made dimensionless by the newly introduced evaporation time t_e to account for differences in drying rates. The evaporation time is

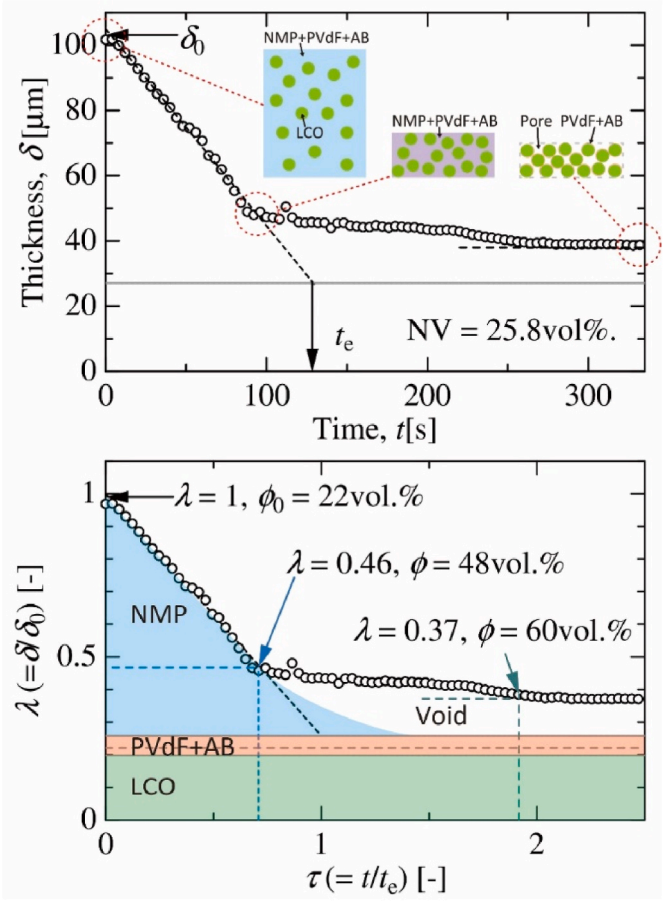

Fig. 4. Typical behavior of the shrinking process of coated slurry and the conversion to the dimensionless plot.

the hypothetical time required for the entire solvent to evaporate while maintaining the drying rate of the concentration period. The reduced time $\tau(=t/t_e)$ indicates the degree of residual solvent in the coating layer but is only valid during the concentration period.

3.2.2. Drying behaviors of AB slurry and LCO slurry

As already mentioned, the cathode slurry is a mixture of LCO particles and AB slurry. When the solvent completely evaporates from the cathode slurry at the end of drying, coarse LCO particles are packed to form the porous main framework of the electrode. On the other hand, the AB slurry is concentrated and dried in the voids. Therefore, in this study, the drying behavior of the LCO and AB slurries was first examined as basic information for understanding the drying behavior of the cathode slurry. Fig. 5 shows the shrinkage behavior of these slurries at drying temperatures of 45 °C and 80 °C. Both slurries initially shrank at a constant rate. The shrinkage rate was found to vary with drying temperature but was not affected by particles.

The concentration period was only observed in the shrinkage behavior of the coated LCO slurry, and the shrinkage ratio decreased to 0.42 and did not change further. The LCO slurry composition in Table 1 shows that the final shrinkage ratio would be 0.244, the total volume of NV components, if a nonporous film had been formed. This difference in shrinkage ratio indicates that LCO particles form a porous structure, and PVdF partially fills the voids. In addition, solvent evaporation was not suppressed by the particle packing because sufficiently large voids were formed within the packed layer of coarse LCO particles. Therefore, it is presumed that the voids were formed after the shrinkage ratio and did not compact further. Furthermore, from the shrinkage ratio, the volume fraction of LCO particles at the end of drying was calculated to be 49 vol %, regardless of the drying temperature. The volume fraction of the random packing layer of non-colloidal spheres ranged from 55 to 63 vol % [29], indicating that the irregular shape of LCO particles increased the void fraction.

On the other hand, the coated AB slurry shrank at a constant rate until its thickness decreased by about 50%, after which the shrinkage rate increased and the shrinkage ratio converged to a constant value. Curiously, the terminal shrinkage rate was greater than the theoretical upper limit of the evaporation rate, the solvent shrinkage rate. This may have been influenced by the lateral transport of NMP. In the case of coarse LCO particles, the lateral transport only caused the drying interface to move laterally through the packed layer of LCO particles toward the center and did not increase the shrinkage rate at the center. In contrast, as the gap between fine AB particles narrows, NMP is efficiently transported both vertically and laterally by the capillary suction flow. Therefore, when the gap between AB particles becomes sufficiently narrow in the latter part of the drying process, the effect of lateral solvent transport becomes significant, and the shrinkage rate locally increases at the thickness measurement point. Note that this shrinkage rate gradually decreased to zero, and the shrinkage ratio of the AB slurry eventually reached about 7 vol%, corresponding to the volume fraction of NV in the AB slurry. This indicates that AB particles-embedded PVdF film was obtained at the end of drying.

The shrinkage behavior of the LCO and AB slurries predicts the packing state of the particles in the cathode film obtained after drying as follows. First, LCO particles produce a packed layer containing voids, the void volume almost the same as that of the LCO particles. On the other hand, the total volume of AB and PVdF in the cathode slurry is 28% of LCO, as shown in Table 1. The AB slurry eventually turns into a nonporous mixture of AB and PVdF. As long as all materials are uniformly dispersed in the cathode slurry throughout the drying process, the mixture of AB particles and PVdF is expected to partially fill the voids between LCO particles, resulting in an ideal particle volume fraction of 64 vol% at the end of drying.

3.2.3. Drying behaviors of cathode slurries

The cathode slurries prepared by the in-parts or in-whole process

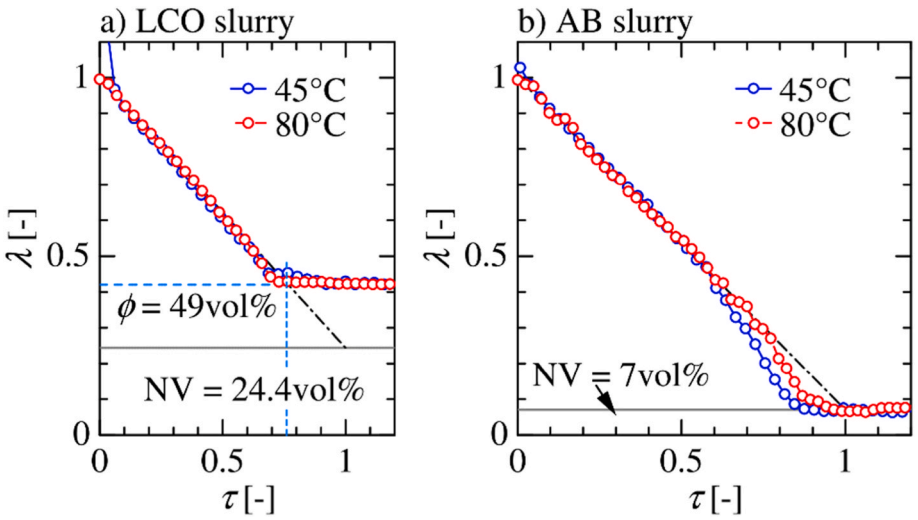

Fig. 5. Shrinking behavior of AB or LCO slurry dried at different drying temperatures.

were coated and dried at 45, 80, and 100 °C. The dimensionless shrinkage behaviors are shown in Fig. 6. The solid gray line in each figure corresponds to $\lambda = 0.258$, indicating the fraction of NV component in the cathode slurry; the measured shrinkage ratio is stable above the solid line because the mixture of AB particles and PVdF partially fills the void between LCO particles.

At 45 °C, the shrinkage rate was initially constant and then increased as in the AB slurry (Fig. 6a). The temporary increase in shrinkage rate was observed due to lateral solvent transport but was not as pronounced as for the AB slurry. At the onset of the temporary rate increase ($\lambda = 0.71$), the solid volume fraction of the AB slurry was concentrated from 2.3 vol% to 3.6 vol%. The volume fraction of LCO particles in the cathode slurry was increased up to 28 vol%. It is thus inferred that LCO particles have not yet formed a packed structure and were embedded in the concentrated AB slurry. Therefore, the effect of lateral drying appeared. However, the coexistence of LCO particles suppressed the degree of the apparent shrinkage rate increase. No difference caused by the slurry preparation process indicates that micro-scale uniformity does not affect the evaporation rate in the concentration period. When the shrinkage ratio λ becomes smaller than 0.43, the film thickness of the in-parts slurry continued to decrease in shrinkage ratio, albeit at a slower rate. In contrast, the in-whole slurry did not shrink any further. At this branching point, the volume fraction of LCO particles in the semi-dry cathode slurry was found to be 47 vol%, equivalent to the random loose packing of spheres (49 vol%). Therefore, after forming the loosely packed structure of LCO particles, the following shrinkage behavior

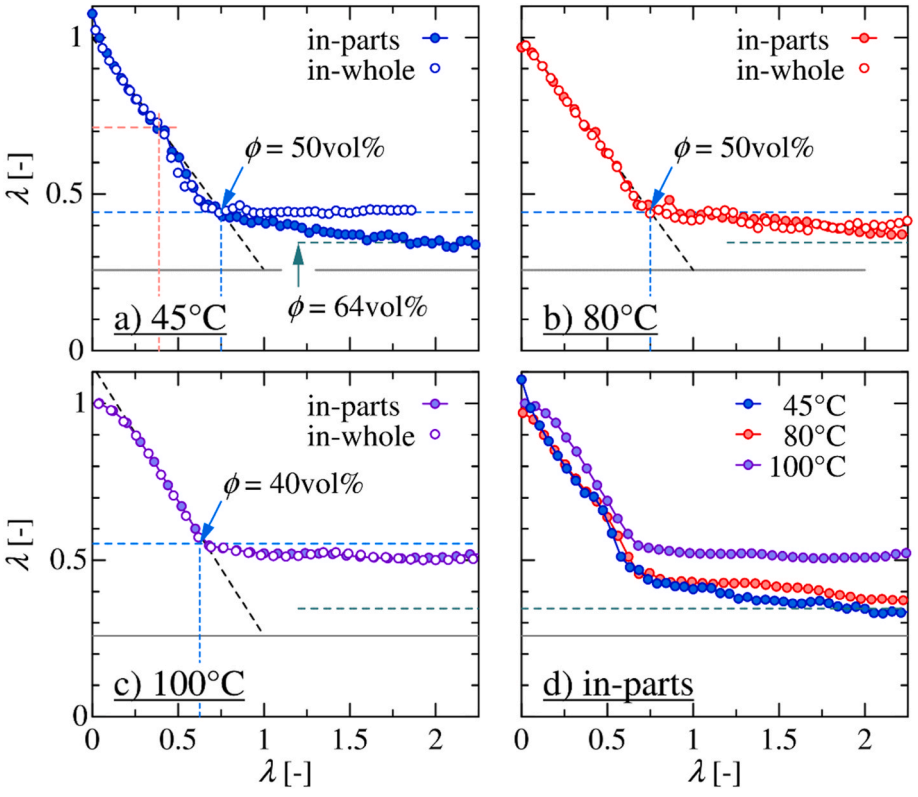

Fig. 6. Effects of the slurry preparation process and drying temperature on the shrinking process of cathode slurry.

depends on the packing state of LCO particles and surrounding AB slurry. From the rheological analysis, it is presumed that LCO particles exist only outside the AB network structure in the in-whole slurry. The packing structure formed by direct contact between LCO particles is not further compressed. Therefore, the concentration of the AB slurry and void formation progressed sequentially in the gap space between LCO particles. On the other hand, for the cathode slurry prepared by the in-parts process, the overall solid volume fraction transitioned from random loose packing (50 vol%) to random close packing (64 vol%). LCO particles in the in-parts cathode slurry were immersed in the AB network structure, allowing LCO particles to rearrange themselves with solvent evaporation, increasing the packing density.

At 80 and 100 °C (Fig. 6 b and c), no temporary increase in the shrinkage rate was observed before the transition from the concentration period to the void formation period. There was no noticeable difference in the shrinkage behavior of the cathode slurries between the in-parts and in-whole slurries at each drying temperature. Furthermore, only at 100 °C, a gradual increase in the shrinkage rate was observed in the very early stage. This is known as a pre-heating period and could not be neglected because it required a relatively long time to elevate the film temperature to a steady value compared to the short drying time at the highest drying temperature.

The results at 45 °C indicate that the packing of LCO particles dominates the initial shrinkage behavior of the cathode slurry. In contrast, the dispersion state of LCO particles in the AB slurry influences the latter shrinkage behavior. As shown in Fig. 6 d, the particle volume fraction at the transition point was 50 vol% for drying temperatures of 45 and 80 °C, and 40 vol% at 100 °C. This suggests that, at 100 °C, LCO particles formed a more loosely packed structure containing a sufficient amount of void to compensate for a considerably large evaporation rate.

At the higher drying temperatures, the slurry preparation process did not affect the subsequent void formation process, despite the different internal structures of cathode slurries. Under drying conditions with a high shrinkage rate, it is presumed that the dispersion state of LCO particles did not affect the packing structure change of LCO particles in the semi-dried AB slurry due to poor mobility of LCO particles in a highly viscous and elastic AB slurry. Additionally, it is assumed that LCO and AB are homogenously concentrated during the concentration period because the effects of LCO particle sedimentation and AB network structure segregation are relatively small. Therefore, the packed layer produced from the in-whole slurry could be compacted during the void formation period. However, LCO particles did not have enough time to rearrange their packing structure at the highest drying rate, and minimal compaction was detected.

3.3. Electrochemical characterization of electrodes

Fig. 7 shows the results of electrochemical tests of battery cells fabricated with electrodes obtained by drying the coated slurries prepared by either process and dried at 45 °C or 80 °C. The top figure plots the discharge capacity at different C rates, and the bottom figure plots the change in discharge capacity versus the number of cycles when repeated charging and discharging at 0.1C. In the rate test, the electrode dried at 80 °C showed greater capacity at all current densities regardless of the slurry preparation process. There was only a slight decrease in capacity with increasing C rate and minor differences between slurry preparation processes. In contrast, electrodes fabricated at 45 °C showed a decrease in discharge capacity, especially under significant C-rate conditions. The capacity decrease was more pronounced for the in-whole slurry. Thus, it was found that slurries with heterogeneously dispersed LCO particles and AB networks at the microscopic scale, dried at low temperatures, did not form sufficient conductive pathways after drying.

On the other hand, the cycle test showed a significant capacity drop compared to the standard measurement. One possible reason is that the electrodes were not pressed in this experiment to extract the drying

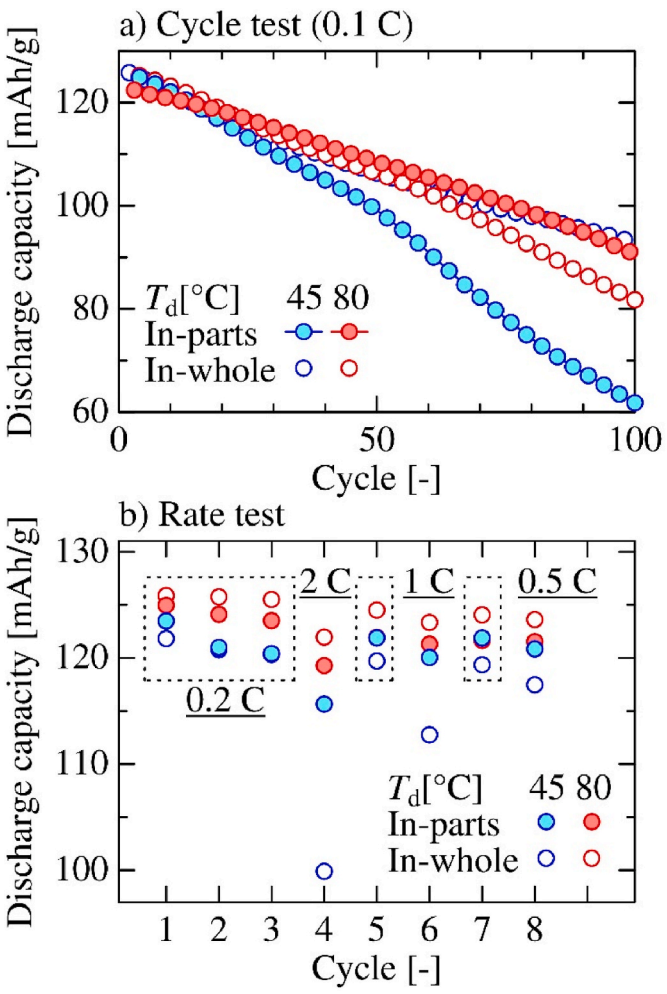

Fig. 7. Electrochemical performance of full cells using cathode films produced from the slurry prepared by different processes and dried at different temperatures.

effect, and sufficient electronic conductivity was not ensured at any of the electrodes. Since the Coulomb efficiency is as low as 95–98%, the effects of film formation and electrolyte decomposition cannot be ignored. However, it is interesting to note that under the same conditions, the drying temperatures for obtaining high cycle characteristics differ between the in-parts and the in-whole slurries. This difference may be attributed to the inhomogeneity of the material in the electrode after drying.

The causes of the differences in electrochemical performance depending on the preparation process and the drying temperature are discussed in terms of the uniformity of material distribution. Fig. 8 shows SEM images of the top and bottom surfaces of the electrode. The image of the bottom surface was taken after the electrode was carefully peeled from the aluminum foil with adhesive tape. The SEM images of the electrode produced by drying in-part slurry at 45 °C indicate that the number density of LCO particles on the top is smaller than that at the bottom. Furthermore, it was also observed that the localization of AB particles on the top. The non-uniform distribution is attributed to the settling of coarse and heavy LCO particles and the segregation of smaller network units of AB particles. Since the AB network structures are fractured into small units in the in-parts cathode slurry, the units are mobile and likely to convey to the drying interface with the evaporation of the solvent. Due to the separation of LCO and AB, it is assumed that the electrochemical reaction occurred unevenly, resulting in the poorest cycle characteristics. Conversely, large AB network structures with low

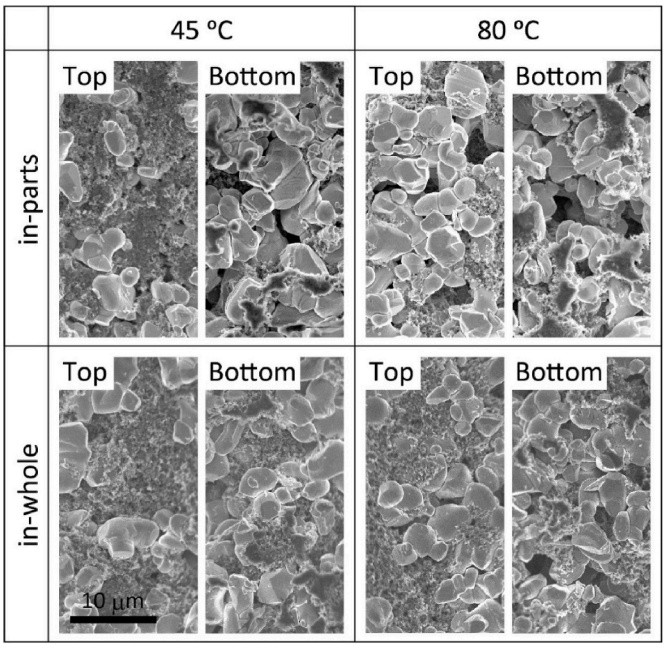

Fig. 8. SEM images at the top and bottom of cathode films.

mobility remained in the in-whole slurry, suppressing AB particle localization. Therefore, it is presumed that the large AB network structure was heterogeneously present in the significant gaps between the loosely packed LCO particles, and the formation of inadequate electric conductive pathways was the cause of the poorest rate characteristics. Based on the above discussion, in porous electrodes, the state of the network of the conductive additives is considered to be dominant in maintaining capacity under high current density. In contrast, the uniformity of conductive additives is considered dominant in maintaining capacity against repeated charging and discharging. At a drying temperature of 80 °C, note that little difference in material distribution between slurry preparation processes was evident, except for the larger voids between the LCO particles.

3.4. Guideline to obtain homogeneous electrodes

From the film shrinkage behavior during drying and the electrochemical properties after drying, it was found that LCO particles must be packed densely and dried so that the AB particles are connected and uniformly distributed in the gaps between them. Therefore, finally, guidelines to avoid inhomogeneous material distribution are discussed. Cardinal et al. proposed a map that predicts the non-uniformity of particle distribution using the Péclet and sedimentation numbers [30]. Brownian diffusive motion, in which thermal fluctuations in a low-viscosity medium essentially homogenize small particles, is essential for maintaining particle uniformity during drying. Péclet number is defined as the ratio of the rate of descent of the drying surface to the rate of diffusion of particles and expressed by the following equation

$$Pe = \frac{hE}{D} = \frac{3\pi\mu dhE}{kT} \tag{1}$$

Herein, D is the diffusion coefficient of particles determined by the Stokes-Einstein equation. E and h are the film shrinkage rate and characteristic length scale, usually initial film thickness, respectively. When the diffusive motion of particles is dominant, i.e., $Pe \ll 1$, particles are uniformly distributed. The Péclet number of LCO or AB primary particles in PVdF solution is calculated as shown in Table 2. This indicates that even if the smallest AB primary particles are dried at the slowest shrinkage rate, the Péclet number is far more extensive than unity, and homogenization by diffusion cannot be expected. AB particles form a network structure that expands throughout the system, as evidenced by their highly elastic behavior. This is a significant factor in the homogeneity of the AB particles during drying.

Table 2
Estimation of Péclet numbers of AB and LCO particles.

Drying temperature		Evaporation rate	Péclet number	
T_d [°C]	T_d [K]	E [m/s]	AB	LCO
45	328	4.6×10^{-8}	5.7×10^{1}	1.1×10^{4}
80	353	5.4×10^{-7}	6.2×10^{2}	1.2×10^{5}
100	373	1.9×10^{-6}	2.1×10^{3}	4.0×10^{5}

$h = 100$ mm, $\mu = 0.17$ Pa s, $k = 1.38 \times 10^{-23}$ J K^{-1}, $d = 35$ nm (AB) or 6.8 μm (LCO).

In contrast, there is essentially no physical mechanism that maintains homogeneity for LCO particles. Therefore, the key to obtaining homogeneous electrodes is avoiding or suppressing the sedimentation of LCO particles. The sedimentation number proposed by Cardinal et al. is the ratio of the terminal settling velocity U of the particle of interest to the shrinkage rate of the drying film, which is introduced to express the competing phenomena of liquid surface lowering and particle sedimentation. Since the concentration of LCO particles is sufficiently high and particles settle in mutual interference with others, the hindered settling velocity proposed by Richardson and Zaki [31] was used to calculate the sedimentation number.

$$N_s = \frac{U}{E} \tag{2}$$

$$U = \frac{\pi d^2 \Delta\rho g}{18\mu}(1-\varphi)^{4.65} \tag{3}$$

Where $\Delta\rho$ is the density difference between the LCO particles and the dispersing medium, the question now arises: what is the dispersing medium for settling LCO particles. The cathode slurry can be viewed as a mixture of LCO particles and AB slurry. However, microscopically, the surface of LCO particles will mostly be in contact with the PVdF solution. The viscosity of the AB slurry varied with the shear rate but was measured in our previous work [24] at shear rates above 0.1 s^{-1}. Assuming that the shear rate related to particle sedimentation is on the order of 0.1 s^{-1} and that the viscosity at that shear rate (170 Pa·s) does not vary with drying temperature, the sedimentation number was calculated as shown in Table 3. From this trial, the sedimentation number of LCO particles based on the AB slurry viscosity is much smaller than unity, indicating that LCO particles do not settle at all and are not suitable for describing the settling behavior of LCO particles. Note that the shear rate near the moving particle surface can be approximated as 10^{-4} s^{-1} by dividing the settling velocity (2×10^{-10} m/s) by the particle radius (3.4×10^{-6} m). The AB slurry viscosity must be much more prominent at the shear rate, resulting in a much smaller sedimentation number. On the other hand, the sedimentation number of LCO particles based on the PVdF solution viscosity clearly shows that the effect of LCO sedimentation appears only at a drying temperature of 45 °C, which is in reasonably good agreement with the experimental facts. Since the viscosity of both AB slurry and PVdF solution increases as drying proceeds, the sedimentation number decreases, and sedimentation stops somewhere during drying.

From the above discussion, a guideline for avoiding electrode heterogeneity was derived. An extensive network structure of AB particles is essential to avoid the migration of AB particles to the drying surface since diffusive motion is ineffective in maintaining AB particle uniformity when the film thickness is on the order of 100 μm. Conversely, to avoid sedimentation of LCO particles, the lowering rate of the drying surface with solvent evaporation must be greater than the settling velocity of the LCO particles calculated using the viscosity of the PVdF solution. The size and volume of voids between LCO particles and the AB network structure in the interstitial spaces must be controlled to

Table 3
Estimation of sedimentation number of LCO particles.

	Viscosity	Terminal velocity	Drying temperature	Evaporation rate	$_{NS}$s (= U/E)
	μ [Pa·s]	U [m/s]	T_d [°C]	E [m/s]	
AB slurry ($0.1s^{-1}$)	170	2.2×10^{-10}	45	4.6×10^{-8}	4.8×10^{-3}
			80	5.4×10^{-7}	4.1×10^{-4}
			100	1.9×10^{-6}	1.2×10^{-4}
PVdF sol. (Newtonian)	0.17	2.2×10^{-7}	45	4.6×10^{-8}	4.8
			80	5.4×10^{-7}	0.41
			100	1.9×10^{-6}	0.12

optimize the high-level manufacturing process of battery electrodes. In the present study, when the drying temperature was too high (100 °C), the film shrinkage during drying was too slight. The electrode film becomes too porous, which probably results in the insufficient formation of conductive pathways. In the future, it is necessary to clarify the process parameters to control the size and volume of voids and conductive path formation during drying.

4. Conclusion

The effects of the slurry preparation process and drying temperature on the internal structure of the cathode film and the electrochemical properties were investigated. The cathode slurry is a mixture of LCO particles and AB slurry, and the preparation process affects their dispersion states. The in-whole process produces a slurry in which LCO particles and AB networks exist independently. In contrast, the in-parts process produces a slurry in which LCO and AB networks are homogeneously distributed on a micro-scale. First, the drying process of the AB or LCO slurry was investigated by employing the film thickness change measurement. The dispersed particles did not affect the shrinkage rate during the initial concentration period. However, the film shrinkage process differed depending on the kinds of dispersed particles as the formation of the packing layer approached. The results suggested that LCO particles form a random close packing structure and that AB slurry is concentrated in the gaps between the LCO particles with void formation. When the in-whole slurry was dried at a slow shrinkage rate, the compaction of the LCO particles layer was suppressed by excessively large AB network structures. The insufficient connection between AB networks after drying resulted in a poor rate performance. On the other hand, LCO particles settled down to the bottom. Smaller AB network units were concentrated at the surface when the in-parts slurry was dried at the same shrinkage rate. The segregation could be explained by the settling velocity of LCO particles affected by the PVdF solution viscosity. As a result, poor cycle performance was observed due to the localization of the electrochemical reaction. In contrast, the electrochemical properties improved at higher drying temperatures, and differences in the slurry preparation process became less apparent. However, at a further higher temperature, due to too large interstitial space between LCO particles, AB conductive pathways are not sufficiently formed. In the actual battery manufacturing process, the electrode is pressed after drying, and the microstructure may be altered. Since this study clarified the dominant factors affecting the microstructure during drying, it is finally possible to examine the effect of the pressing process on battery performance.

CRediT authorship contribution statement

Yoshiyuki Komoda: Conceptualization, Methodology, Writing – original draft, Visualization. **Kaoru Ishibashi:** Investigation, Data curation. **Kentaro Kuratani:** Conceptualization, Writing – review & editing. **Kosuke Suzuki:** Validation. **Naoto Ohmura:** Funding acquisition. **Hironori Kobayashi:** Supervision.

Declaration of competing interest

The authors declare the following financial interests/personal relationships which may be considered as potential competing interests: Naoto Ohmura reports financial support was provided by Japan Society for the Promotion of Science.

Data availability

Data will be made available on request.

Acknowledgment

This work was supported by the Japan Society for the Promotion of Science (JSPS) KAKENHI Grant number JP19KK0127. This study has been conducted under the cross-appointment framework between Kobe University and AIST. The authors are grateful for the opportunity to have collaborated under this framework.

References

[1] B.P.N. Nguyen, S. Chazelle, M. Cerbelaud, W. Porcher, B. Lestriez, Manufacturing of industry-relevant silicon negative composite electrodes for lithium ion-cells, J. Power Sources 262 (2014) 112–122.
[2] L. Zhang, Y. Liu, B. Key, S.E. Trask, Z. Yang, W. Lu, Silicon nanoparticles: stability in aqueous slurries and the optimization of the oxide layer thickness for optimal electrochemical performance, ACS Appl. Mater. Interfaces 9 (2017) 32727–32736.
[3] Z. Karkar, D. Guyomard, L. Roué, B. Lestriez, A comparative study of polyacrylic acid (PAA) and carboxymethyl cellulose (CMC) binders for Si-based electrodes, Electrochim. Acta 258 (2017) 453–466.
[4] L.H. Huang, C.C. Li, Effects of interactions between binders and different-sized silicons on dispersion homogeneity of anodes and electrochemistry of lithium-silicon batteries, J. Power Sources 409 (2019) 38–47.
[5] W.B. Hawley, J. Li, Electrode manufacturing for lithium-ion batteries—analysis of current and next generation processing, J. Energy Storage 25 (2019), 100862.
[6] L.S. Kremer, A. Hoffmann, T. Danner, S. Hein, B. Prifling, D. Westhoff, C. Dreer, A. Latz, V. Schmidt, M. Wohlfahrt-Mehrens, Manufacturing process for improved ultra-thick cathodes in high-energy lithium-ion batteries, Energy Technol. 8 (2020), 1900167.
[7] Y. Liu, R. Zhang, J. Wang, Y. Wang, Current and future lithium-ion battery manufacturing, iScience 24 (2021), 102332.
[8] Y.S. Zhang, N.E. Courtier, Z. Zhang, K. Liu, J.J. Bailey, A.M. Boyce, G. Richardson, P.R. Shearing, E. Kendrick, D.J.L. Brett, A review of lithium-ion battery electrode drying: mechanisms and metrology, Adv. Energy Mater. 12 (2022), 2102233.
[9] E. Ayerbe, M. Berecibar, S. Clark, A.A. Franco, J. Ruhland, Digitalization of battery manufacturing: current status, challenges, and opportunities, Adv. Energy Mater. 12 (2022), 2102696.
[10] W. Pfleging, Recent progress in laser texturing of battery materials: a review of tuning electrochemical performances, related material development, and prospects for large-scale manufacturing, Int. J. Extrem. Manuf. 3 (2020), 012002.
[11] Z. Hu, J. Hao, D. Shen, C. Gao, Z. Liu, J. Zhao, B. Lu, Electro-spraying/spinning: A Novel Battery Manufacturing Technology, Green Energy & Environment, 2022 in Press.
[12] T. Chu, S. Park, K. Fu, 3D printing-enabled advanced electrode architecture design, Carbon Energy 3 (2021) 424–439.
[13] C.-C. Li, Y.-W. Wang, Binder distributions in water-based and organic-based LiCoO2 electrode sheets and their effects on cell performance, J. Electrochem. Soc. 158 (12) (2011) A1361–A1370.
[14] S. Lim, K.H. Ahn, M. Yamamura, Latex migration in battery slurries during drying, Langmuir 29 (2013) 8233–8244.
[15] S. Jaiser, M. Müller, M. Baunach, W. Bauer, P. Scharfer, W. Schabel, Investigation of film solidification and binder migration during drying of Li-Ion battery anodes, J. Power Sources 318 (2016) 210–219.

[16] F. Font, B. Protas, G. Richardson, J.M. Foster, Binder migration during drying of lithium-ion battery electrodes: modelling and comparison to experiment, J. Power Sources 393 (2018) 177–185.
[17] K.M. Kim, W.S. Jeon, I.J. Chung, S.H. Chang, Effect of mixing sequences on the electrode characteristics of lithium-ion rechargeable batteries, J. Power Sources 83 (1–2) (1999) 108–113.
[18] G.-W. Lee, J.H. Ryu, W. Han, K.H. Ahn, S.M. Oh, Effect of slurry preparation process on electrochemical performances of LiCoO2 composite electrode, J. Power Sources 195 (18) (2010) 6049–6054.
[19] V. Wenzel, N. Hermann, N. Dorit, Challenges in lithium-ion-battery slurry preparation and potential of modifying electrode structures by different mixing processes, Energy Technol. 3 (7) (2015) 692–698.
[20] K. Alexander, Y. Ein-Eli, Conveying advanced Li-ion battery materials into practice the impact of electrode slurry preparation skills, Adv. Energy Mater. 6 (21) (2016), 1600655.
[21] K. Konda, S.B. Moodakare, P.L. Kumar, M. Battabyal, J.R. Seth, V.A. Juvekar, R. Gopalan, Comprehensive effort on electrode slurry preparation for better electrochemical performance of LiFePO4 battery, J. Power Sources 480 (2020), 228837.
[22] K. Huber, A. Adam, D. Grießl, A. Kwade, Understanding slurry mixing effects on the fast charging capability of lithium-ion battery cells: Methodology and case study, J. Power Sources 536 (2022), 231455.
[23] K. Kuratani, K. Ishibashi, Y. Komoda, R. Hidema, H. Suzuki, H. Kobayashi, Controlling of dispersion state of particles in slurry and electrochemical properties of electrodes, J. Electrochem. Soc. 166 (2019) A501.
[24] Y. Komoda, K. Ishibashi, K. Kuratani, R. Hidema, H. Suzuki, H. Kobayashi, Rheological interpretation of the structural change of LiB cathode slurry during the preparation process, JCIS Open 5 (2022), 100038.
[25] Y. Komoda, R. Kimura, K. Niga, H. Suzuki, Formation of particle layer within coated slurry characterized by thickness variation, Dry. Technol. 29 (9) (2011) 1037–1045.
[26] Y. Komoda, K. Niga, H. Suzuki, Effect of shear strain applied in coating and colloidal stability on the drying process of latex dispersions, J. Chem. Eng. Jpn. 48 (1) (2015) 87–93.
[27] Y. Komoda, S. Kobayashi, H. Suzuki, R. Hidema, Effect of shear strain in coating on the particle packing of gelled-clay particle dispersions during drying, J. Coating Technol. Res. 12 (2015) 939–948.
[28] Irvin M. Krieger, Thomas J. Dougherty, A mechanism for non-Newtonian flow in suspensions of rigid spheres, Trans. Soc. Rheol. 3 (1) (1959) 137–152.
[29] Z. Francesco, Mathematical physics: packings close and loose, Nature 453 (7195) (2008) 606.
[30] C.M. Cardinal, Y.D. Jung, K.H. Ahn, L.F. Francis, Drying regime maps for particulate coatings, AIChE J. 56 (11) (2010) 2769–2780.
[31] J.F. Richardson, W.N. Zaki, Sedimentation and fluidization: Part I, Trans. Inst. Chem. Eng. 32 (1954) S82–S100.